forests

MDPI

Article

A Novel Method of Boreal Zone Reforestation/Afforestation Estimation Using PALSAR-1,2 and Landsat-5,8 Data

Valery Bondur [1,*], Tumen Chimitdorzhiev [2], Irina Kirbizhekova [2] and Aleksey Dmitriev [2]

[1] AEROCOSMOS Research Institute for Aerospace Monitoring, 105064 Moscow, Russia
[2] Institute of Physical Materials Science of SB RAS, 670047 Ulan-Ude, Russia; tchimit@ipms.bscnet.ru (T.C.); kirbizhekova@ipms.bscnet.ru (I.K.); dav@ipms.bscnet.ru (A.D.)
* Correspondence: vgbondur@aerocosmos.info

Abstract: Nowadays, global remote sensing studies of tropical forest parameters are relevant for assessing carbon sequestration, whereas boreal forests receive little attention. This is due to the current idea that forests with greater aboveground biomass absorb more carbon. However, new research indicates that rapidly growing young forests take up more carbon than mature ones. Therefore, it is necessary to develop universal methods of remote reforestation/afforestation monitoring. The existing reforestation methods rely on the separate analysis of multispectral optical images and radar data. Here, we propose a method for analyzing the joint dynamics of NDVI (or the Normalized Burn Ratio, NBR) and the radar vegetation index (RVI) on a 2D plot for a test reforestation site. NDVI and NBR time series were derived from Landsat-5,8 data, and the RVI was derived from ALOS-1,2 and PALSAR-1,2 for 2007–2020 using the resources of Google Earth Engine. The quantitative parameters to evaluate the degree of reforestation and changes in the species composition of young trees have been suggested. The suggested method enables a more thorough evaluation of reforestation by measuring the coupled dynamics of the projective cover of young trees and aboveground biomass.

Keywords: boreal zone reforestation/afforestation; NDVI; Landsat time series; radar vegetation index; ALOS-1/2 PALSAR-1/2; Google Earth Engine

check for updates

Citation: Bondur, V.; Chimitdorzhiev, T.; Kirbizhekova, I.; Dmitriev, A. A Novel Method of Boreal Zone Reforestation/Afforestation Estimation Using PALSAR-1,2 and Landsat-5,8 Data. *Forests* **2024**, *15*, 132. https://doi.org/10.3390/f15010132

Academic Editor: Tianxiang Yue

Received: 27 October 2023
Revised: 1 January 2024
Accepted: 5 January 2024
Published: 8 January 2024

Copyright: © 2024 by the authors. Licensee MDPI, Basel, Switzerland. This article is an open access article distributed under the terms and conditions of the Creative Commons Attribution (CC BY) license (https://creativecommons.org/licenses/by/4.0/).

1. Introduction

The carbon balance assessment is one of the pressing worldwide issues related to the study of climate change. At present, various models that predict positive or negative carbon balance in the year 2100 have been developed. Various estimates of forest-absorbing capacity are being made based on these models [1,2]. For example, [3] shows the absence of appreciable changes in carbon sinks before and after forest thinning and after selective logging. It was determined in [4] that carbon absorption by mature tropical and boreal forests in Siberia averages 0.85 Pg/year (1 Pg = 10^{15} g = 10^{12} kg), and in young forests it is 1.30 Pg/year. In [5], using the example of Latin America, a significant role of forest regrowth is also confirmed. After clear cuttings, young forests enable the active accumulation of carbon in aboveground biomass, thereby partially balancing carbon emissions as a result of burning fossil fuels, forest degradation, and other anthropogenic sources. In addition, in [6], it is shown that forests located on agricultural lands are of greater importance for the absorption of greenhouse gases: 1 hectare of forest land on average absorbs about 1 ton of greenhouse gases per year, and 1 hectare of protective and anti-erosion forests on agricultural land absorbs about 7 tons per year, i.e., seven times more.

Thus, the urgency of reforestation is increasing [7,8]. There is a viewpoint [8] that one of the most promising ways to quickly sequester carbon from the atmosphere is through the restoration of tropical forests. This suggestion should cover all forests on the planet. First of all, it is necessary to evaluate the reforestation potential of a significant area of burned Siberian boreal forests [9,10]. This is relevant because during their growth, young

trees absorb more carbon than mature forests. Therefore, it is necessary to quantify the area covered by young trees, their species composition, and the time of recovery in a mature forest. The criterion for the latter is suggested to be the point in time after which the remotely determined basic parameters of the forest, i.e., the leaf area index and biomass, will stop changing.

The purpose of this effort is to develop a new method for remote reforestation/afforestation assessment, taking into account the above.

Since this is an empirical method, the following structure of the article is proposed: there are six sections in this article. Section 2 retrospectively covers some related works. The next section is the study area and materials. Section 4 introduces the empirical method that we proposed in detail. The comparison of results and discussion are carried out in Section 5. The conclusions are presented in Section 6.

2. Related Works

In a recent study [11], a global map of the spatial distribution of natural and managed reforestation processes was created based on different time series of remote sensing data. An analysis of these data (as of 2015) showed the difference in results due to the different spatial resolutions of MODIS (250 m) and Landsat (30 m) data. Similar work using MODIS, Landsat-5,8, and Sentinel-2 data has also been conducted in Russia [9,10,12]. This is relevant given the large areas of boreal forests in Siberia. In [10], optical data from Russian satellites Kanopus-V, Resurs-P, Meteor-M, Electro-L, and Arktika-M series are also used for the assessment of areal forest changes [9,10,12]. Generally, such an approach that involves optical data [9–12] actually shows a change in the projective cover of forest vegetation, which is associated with the reflection of solar radiation from its overstory. However, changes in the aboveground biomass of trunks and branches are not taken into account in this case.

At the same time, remote forest monitoring systems are being developed based on the processing of Big SAR data [13–16]. The main advantage of radar data is the high penetrating power of radio waves. An L-band makes it possible to evaluate a significant part of the aboveground biomass of trees.

As discussed above, estimating biomass changes can be one of the parameters that quantify carbon sequestration by forests around the planet. However, as one can see on the web page of the JICA-JAXA Forest Early Warning System in the Tropics (JJ-FAST) [13]:

> "*JJ-FAST is a web-based system using JAXA's ALOS-2 to monitor tropical forests in 78 countries every 1.5 months and release deforestation data, even in the rainy season. Users can easily access the data for deforested areas from PCs and mobile devices and download the data*".

Additionally, JJ-FAST does not control managed forests or the natural reforestation processes, but this is relevant for boreal Siberian forests.

Ref. [16] suggested a methodology of combined use of fully polarimetric L-band satellite radar data to assess the temporal dynamics of an increase in volume inhomogeneity (trunk and branches) and analyze a long NDVI time series. Generally, there are many methods to analyze fully polarimetric radar data that are potentially suitable and promising for such studies. However, this assumes (1) that fully polarimetric radar data are available, which is problematic due to the lack of such long-term continuous time series, and (2) that dedicated software and certain knowledge in this area are available. All this makes their use difficult.

Recently, with advances in cloud technologies, methods for online processing and remote sensing data analysis to assess reforestation have been developed [17–19]. For example, [17] used Landsat best-available-pixel (BAP) composites as input data to calibrate the random forest classification model and classify afforestation between 1985 and 2019. The BAP procedure was implemented in 2021 in Google Earth Engine (GEE), and the code is openly available [20]. Since these works [17–22] also involve Landsat data similar

to [9–12], the main shortcoming of this method is its inability to remotely assess changes in the aboveground biomass volume.

Thus, the existing methods for evaluating data produced by satellite forest monitoring systems can be divided into the following categories:

- Multispectral optical imagery analysis methods (including online and cloud-based ones) to assess the species composition and projective forest cover, including to detect cutting, reveal various anomalies based on spectral characteristics, etc. [9–12,17–19];
- Polarimetry and interferometry radar data analysis methods, mostly L-bands, to assess aboveground forest vegetation biomass, forest canopy height, etc. [13–15];
- Combined optical and microwave data use methods for a comprehensive analysis of forest parameters [16].

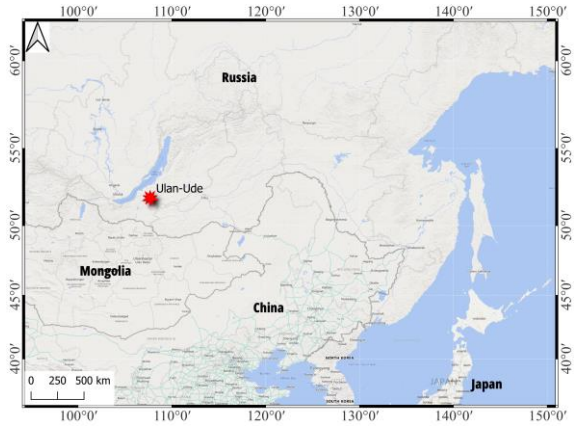
Along with the above methods' shortcomings listed in [9–19], most of the methods (except for [17–19]) involve significant satellite data archives, computational resources, and appropriate software. Moreover, state-of-the-art research suggests that the results of a global assessment should be publicly accessible via the Internet and reproducible by other researchers. These are the basic requirements that should be considered for the satellite monitoring of reforestation (both natural and intentional), including Siberian boreal forests.

3. Study Area and Materials

3.1. Study Area

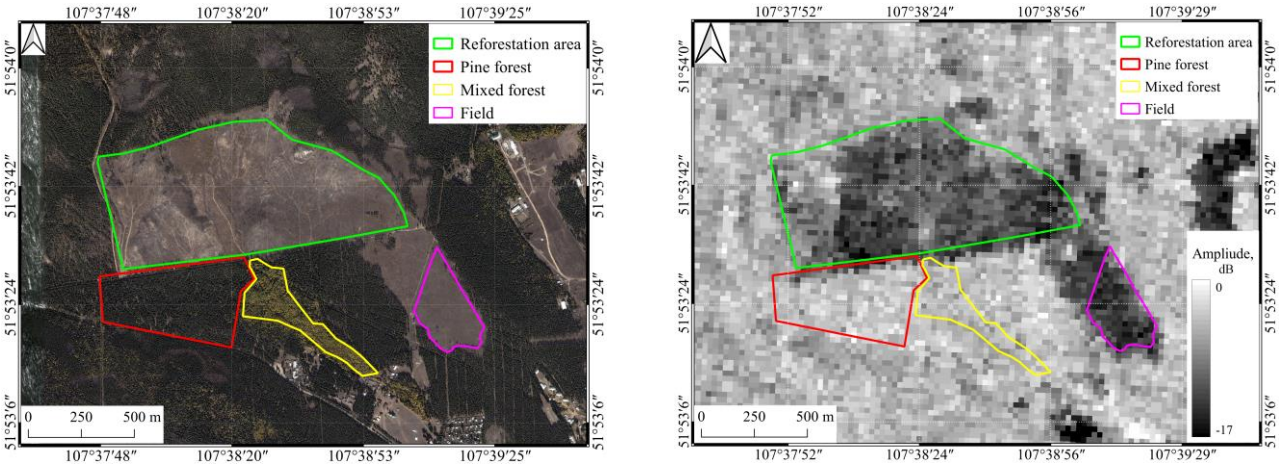
The same area was used as a reforestation test site as in [16]. The test site is a typical area of Siberian boreal forests located in Russia, not far (82 km) from the Baikal Lake, a UNESCO World Heritage area, near the city of Ulan-Ude (107.64° N, 51.90° E). The terrain is mountainous, with 680–800 m elevations and slopes up to 30°. In 2003, a strong wildfire completely destroyed 69 ha of forest. After the forest fire, pine seedlings (*Pínus sylvéstris*) were planted in the lowlands and on smooth slopes. Natural reforestation takes place in the remaining territory.

Figure 1 shows the location and scheme of the reforestation area (RA) (green polygons in Figure 1b) and three reference areas (21.9, 14, and 8.9 ha). At present, the age of young stock varies from 1 to 19 years, and its height does not exceed 4 m. Within the first reference area, there is a pine forest (PF) (red polygons in Figure 1b) similar to the forest of the study area in the pre-fire period. The second reference area (yellow polygons in Figure 1b) is a mixed forest (MF) with the following species composition: larch (65%), birch (32%), and pine (3%). The open treeless area is marked with a magenta contour (polygons in Figure 1b) and labeled as a "Field". Figure 2a shows a photograph of a reforestation site (in the foreground) and a reference site of a mature coniferous forest (in the background). Figure 2b presents a mixed forest picture.



(**a**)

Figure 1. *Cont.*



(**b**) (**c**)

Figure 1. (**a**) The study area location (red asterisk); (**b**) locations of the reforestation and reference areas (Google Earth, September 2007); (**c**) ALOS-1 PALSAR-1 annual mosaic with the reforestation and reference areas (July 2007).



(**a**) (**b**)

Figure 2. Test site photos: (**a**) the reforestation site and reference pine forest, (**b**) mixed forest.

3.2. Materials

3.2.1. Landsat Data

The values of the NDVI, NBR, and RVI averaged over the territory of the four indicated areas were used for the analysis. NDVI values averaged over 32-day periods according to Landsat-5 [23] and Landsat-8 [24] for the period of 2007–2020 were obtained directly from the GEE catalog. The selection and subsequent averaging of NDVI over the winter period (with snow cover) makes it possible to level out the influence of green grass, fast-growing shrubs, and soil when assessing long-term changes in NDVI for deciduous trees (trunks and branches against the snow) and evergreen pines. It should be noted that against the background of unchanging white snow (NDVI is close to zero), winter mixed forest NDVI (positive NDVI no more than 0.2) describes the projective coverage by trunks and branches without green foliage (larch needles), and in fact, this parameter will be compared with

forest undergrowth NDVI. In the same way, NBR values [23] were compared with NDVI data. The NBR is calculated according to the following equation [24]:

$$\mathrm{NBR} = \frac{\mathrm{NIR} - \mathrm{SWIR}}{\mathrm{NIR} + \mathrm{SWIR}} \quad (1)$$

where NIR and SWIR are the surface reflectance values in the near- and short-wave infrared bands, respectively (0.85–0.90 μm and 1.55–1.75 μm). As a matter of fact, the names of indices obtained using this equation differ, so a generalization is made in [25].

3.2.2. ALOS-1,2 PALSAR-1,2 Data

The dual polarization radar vegetation index, RVI, based on ALOS-1,2 and PALSAR-1,2 [26] data was calculated by GEE according to the following equation [25]:

$$\mathrm{RVI} = \frac{4\gamma^0_{\mathrm{HH}}}{\gamma^0_{\mathrm{HH}} + \gamma^0_{\mathrm{HV}}}, \quad (2)$$

where γ^0_{HH}, γ^0_{HV} are radiometrically normalized radar backscattering values at horizontal (HH) and cross (HV) polarizations, respectively.

Radar data on the GEE web resource are annual image mosaics obtained for a specified date. For our test site ALOS-1, PALSAR-1 data for 2007-07-23, 2008-06-09, 2009-09-12, and 2010-06-15 (yyyy-mm-dd) and ALOS-2 PALSAR-2 for 2015-02-25, 2016-06-15, 2017-10-04, 2018-07-25, 2019-07-24, and 2020-07-22 (yyyy-mm-dd) were available [27]. The RVI was calculated over all the above dates, except for 25 February 2015. This is because seasonal soil and vegetation freezing/thawing processes greatly affect the radar backscattering value, γ^0 [28,29]. Therefore, same-season radar data are to be used. In our case, this is a period of stable positive temperatures.

4. Proposed Method and Results

4.1. Description of the Method

The method is divided into three main parts, as shown in Figure 3. At the first stage, NDVI, NBR, and RVI time series were obtained for all four sites (treeless, mixed forest, coniferous, and the reforestation site (see Figure 1b,c) using Google Earth Engine (GEE) (see the Google Earth Engine box in Figure 3). Next, these time series are considered together on two-dimensional NDVI (abscissa), RVI (ordinate), and NBR (abscissa) and RVI (ordinate) planes (see the NDVI-RVI box in Figure 3). In this case, three time series, except for reforestation site data, are approximated by the following points: the origin of a two-dimensional plane corresponds to the treeless site, and the reference sites of mixed and coniferous mature forests are the corresponding two points in the first quadrant (positive index values). These three points form a triangle, within which the dynamics of the fourth time series, i.e., the reforestation area, are considered (see the DRI and RSI boxes in Figure 3). Two new values are introduced that characterize (1) the degree of reforestation (simultaneous increase in projective cover and aboveground biomass) and (2) the degree of species composition similarity to a mixed or coniferous forest. Finally (see the last two boxes in Figure 3), we obtain the predicted reforestation time and species composition.

Let us address the plot in Figure 3 in more detail. As is known, NDVI allows for assessing the degree of areal greenness of a vegetation region. This projective green vegetation cover increases in the case of reforestation.

In our case, we address winter periods, so we obtain data on an increase in young forest coverage compared to reference areas of mixed and coniferous forests, while the spectral response for NDVI in a winter period is formed by branches of deciduous young forest and evergreen pine needles. The NBR characterizes the degree of charring of forest debris and soil after a forest fire.

Note that NBR values close to 0 denote completely burned and charred forests, and values close to 1 correspond to forests unaffected by fire, or, in our case, completely recovered after it.

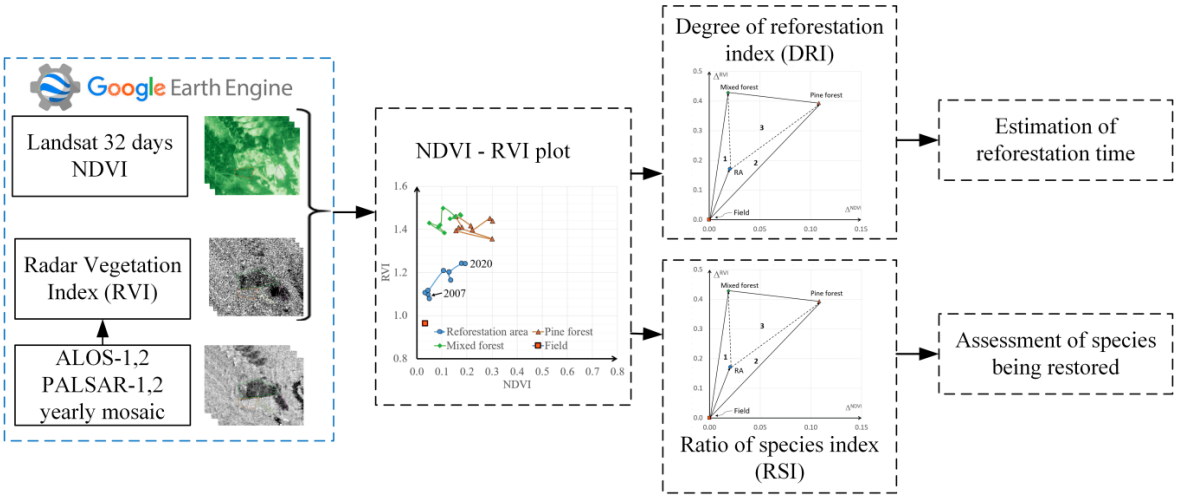


Figure 3. Method workflow.

NDVI and NBR calculation equations (see Equation (1)) are identical: spectral brightness in red or short-wave infrared bands, respectively, is compared to NIR. In the red spectral band, intense absorption occurs by chlorophyll, and in the short-wave IR band, water is absorbed. Thus, NDVI allows us to assess the chlorophyll content, and the NBR gives information on water content (humidity) or the lack of water in plants. In general, these indices are similar in principle, but the effectiveness of reforestation monitoring is expedient to compare.

Since the fire occurred in 2003 and we analyzed the period 2007–2020, we can expect a certain positive trend in all three indices: the NDVI, NBR, and RVI. However, the radar index dynamics depend on the increase in the number of trunks and branches commensurable to the L-band wavelength (24 cm). Thus, the NDVI-RVI and NBR-RVI relationships are to be compared in pairs.

Let us consider the time series of vegetation indices for reference forest areas and the treeless area, as well as the area of post-fire reforestation. Two charts are built as follows:

- RVI vs. average winter NDVI (Figure 4a);
- RVI vs. average winter NBR (Figure 4b).

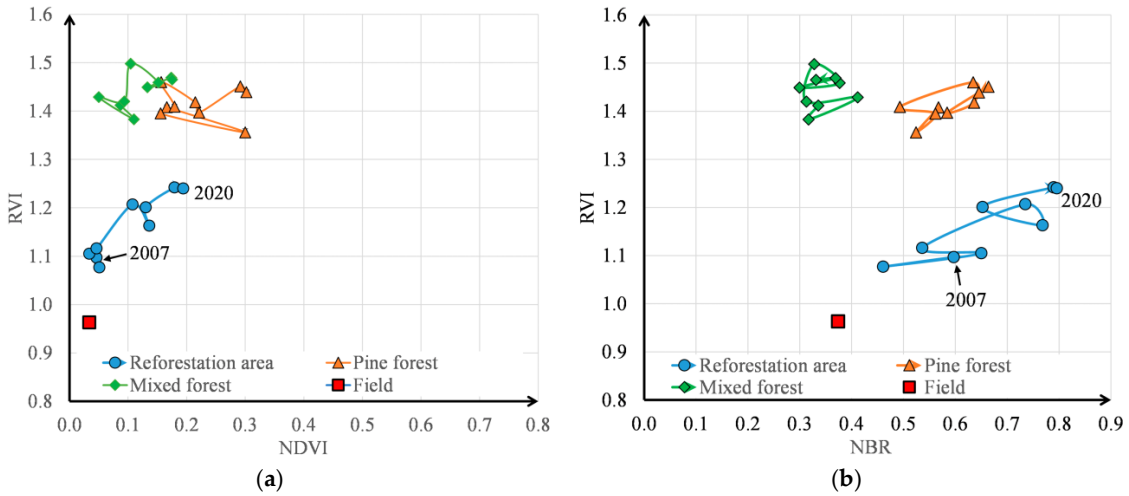


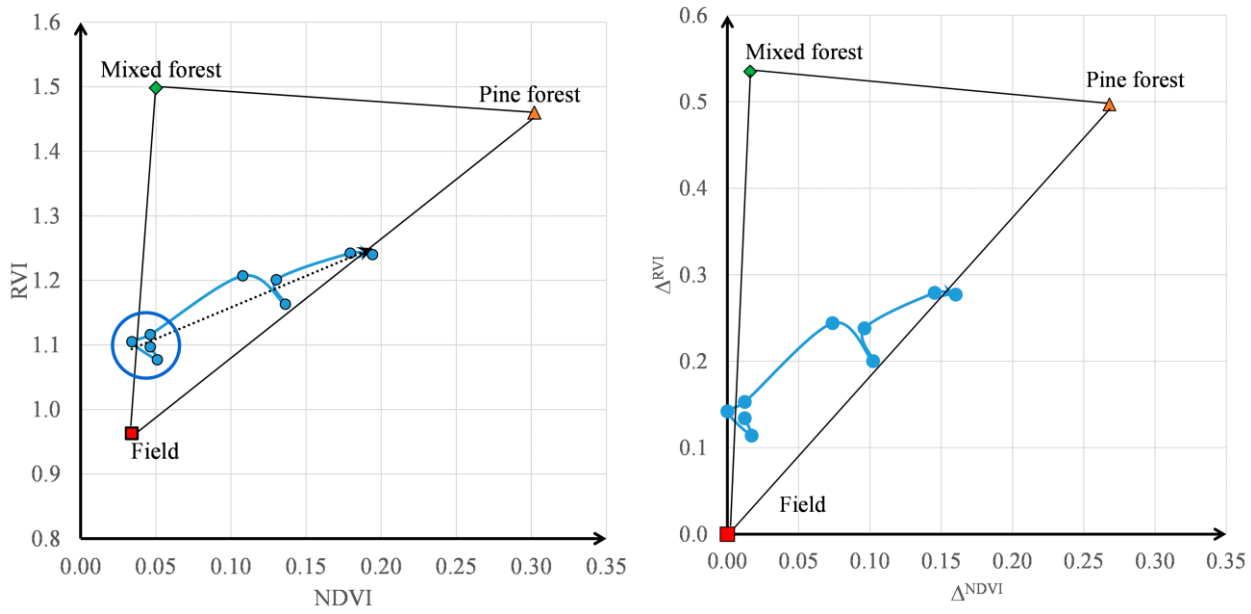
Figure 4. A 2D distributions of the time series: (**a**) NDVI-RVI and (**b**) NBR-RVI.

The red square in Figure 4 denotes a treeless area. The minimal vegetation indices of the field and the reforestation site were selected as this point's coordinates. It was assumed that these minimal values corresponded to the real conditions of the field at the beginning of the time series, with a certain roughness of the soil cover. The distance from this point to the origin characterizes the deviation of an actual terrain from the ideal case, i.e., an absolutely smooth plain without vegetation.

Changes for the studied reference sites are shown in Figure 4 as curves of a moving average with a frequency of 2. This shows actual fluctuations around an average value. Generally, it means the temporal stability of reference areas of mixed and coniferous forests. Therefore, we suggest considering the indices for these reference areas as constants and representing them as two points. To account for all values in both time series, the following was performed:

- A point in the reference mixed forest was assigned minimum NDVI and NBR values in the X-direction and maximum RVI values in the Y-direction;
- A point in the reference coniferous forest was assigned maximum NDVI and NBR values in the X-direction and minimum RVI values in the Y-direction.

Thus, the totality of all three reference sites (the treeless smooth site, mixed and coniferous forests) makes a triangle area in Figure 5a. It is suggested to address the reforestation dynamics inside this triangle. However, the 2D NBR-RVI distribution does not fit in such a graphic model.



(**a**) (**b**)

Figure 5. The reforestation dynamics graphic model with linear trend (dotted line) (**a**) and the origin shifted to the "Field" point (**b**).

Expected reforestation options with linear and other types of approximations are already directed beyond this triangle at the initial stage. This is due to the fact that the NBR [22,23] was originally intended to assess the degree of charring in a forest damaged by a fire. The NBR actually allows us to estimate the relative water content (1.5–1.6 µm water absorption band). Therefore, after a while, even in cases of complete forest and soil burning, the degree of charring changes, and the fertile soil layer and vegetation begin to recover. Vegetation recovery should be assessed using vegetation indices, which are to be calculated using the red and near-IR spectral band ranges. So, further, only NDVI and RVI distributions will be considered.

In the time period 2007–2010, the study area track points were grouped in a small zone of the initial stage of growth (see the blue circle). On average, NDVI values for this period corresponded to the treeless site value (the "Field" point in Figure 5a), and the RVI was higher by 0.136 compared with treeless areas. The latter was probably due to the higher roughness of the afforestation site and significant terrain impact (the incident angle of radar backscattering varied between 25° and 50°).

For convenience, we placed the origin at the "Field" point (Figure 5b), and the abscissas and ordinates were the differences between the relevant vegetation indices:

$$\Delta_i^{\mathrm{NDVI}} = \mathrm{NDVI}_i - \mathrm{NDVI}_{Field}, \tag{3}$$

$$\Delta_i^{\mathrm{RVI}} = \mathrm{RVI}_i - \mathrm{RVI}_{Field}, \tag{4}$$

where the *i* subscript means one of forest or reforestation sites.

4.2. Quantitative Reforestation Assessment

The position of the "reforestation site" point inside the triangular zone in Figure 6 characterizes the average recovery 15 years after the fire. A vector that begins at the origin and is pointed to the "reforestation area" point shows the average dynamics for the years 2007–2020. Vectors denoted by dashed lines limit the area of future growth to pine, a mixed forest, or an intermediate one.

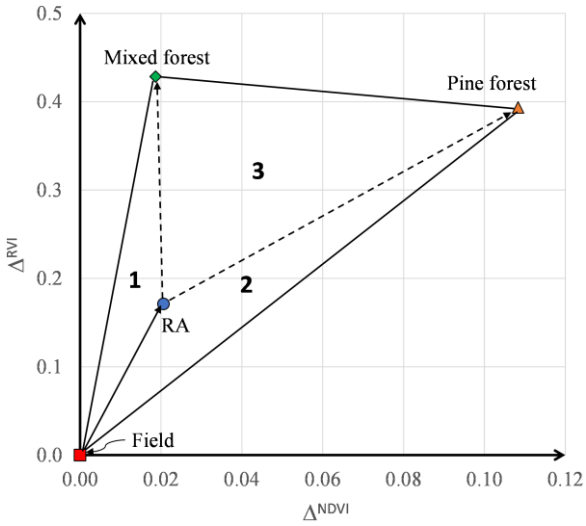


Figure 6. Graphic interpretation of reforestation dynamic. RA = reforestation area.

For the quantitative assessment of the degree of reforestation, we used the ratio of the areas of small triangles 1, 2, and 3 and the big triangle, whose vertices are reference points (see Figure 6). As the forest recovers, the area of triangle 3 will decrease, and the total area of triangles 1 and 2 will increase. Let us introduce a quantitative reforestation indicator, the degree of reforestation index (DRI), which is equal to the ratio of the sum of the areas of triangles 1 and 2 to the total area of reforestation, *S*:

$$\mathrm{DRI} = \frac{s_1 + s_2}{S} = \left(1 - \frac{s_3}{S}\right);\ S = s_1 + s_2 + s_3 \tag{5}$$

where s_1, s_2, and s_3 are the areas of small triangles 1, 2, and 3 and S is the area of the big triangle. The DRI ≈ is 0 after the fire when vegetation is completely burned, and the DRI approaches 1 after reforestation is complete. The area of triangles on a plane can be calculated using the formulas of analytical geometry, knowing the coordinates of their

vertices. For example, for triangle 1, the area is defined as the value of the determinant of a matrix composed of the coordinates of its vertices:

$$s_1 = \mp\frac{1}{2}\begin{vmatrix} \Delta_{MF}^{\mathrm{NDVI}} & \Delta_{MF}^{\mathrm{RVI}} \\ \Delta_{RA}^{\mathrm{NDVI}} & \Delta_{RA}^{\mathrm{RVI}} \end{vmatrix} \quad (6)$$

A positive or negative sign is selected based on the need for a positive area value.

Restoration or substitution of the species composition may be assessed using the ratio of triangles s_1 and s_2 areas. The more pine trees there are in the reforestation area, the greater s_1 will be and the less s_2 will be. For a quantitative assessment of the pine share (or other principle species), let us introduce the ratio of species index (RSI), which is the ratio of the area of triangle 1 to the sum of the areas of triangles 1 and 2:

$$\mathrm{RSI}_{pine} = \frac{s_1}{s_1 + s_2} \quad (7)$$

The RSI_{pine} at the early reforestation stage mostly characterizes the percentage of the territory covered by young pines. Further, in the case of crown closure, this indicator means the share of pines in the species composition. It varies from 0 when the main species is completely replaced by deciduous ones to 1 when a pine forest is completely restored.

5. Separate Assessment for NDVI/RVI and Discussion

Let us compare the obtained result with the NDVI and RVI time series analyses for all four sites (Figure 7). Additionally, linear trends of the relevant data series are given for better visualization. The rate of NDVI increase for the reforestation site is 3.05- and 5.74-fold higher than mature mixed and pine forests, respectively.

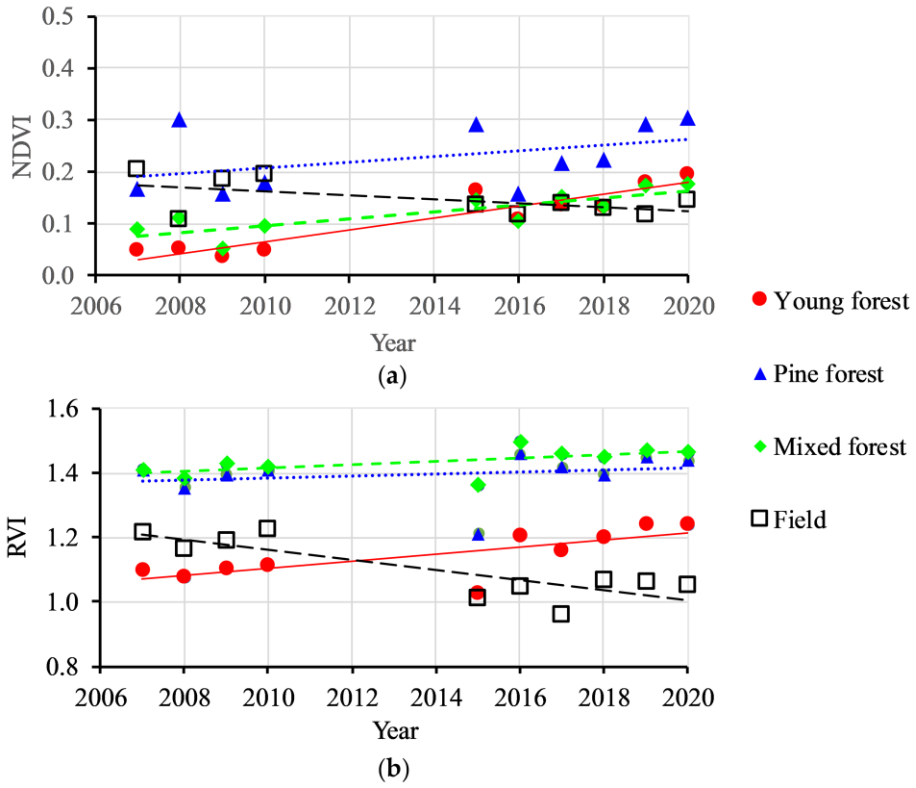


Figure 7. Vegetation index time series and trends: (**a**) 2007–2020 Landsat-5,8-based winter NDVI; (**b**) 2007–2020 ALOS-1,2 PALSAR-1,2-based RVI.

The significance and reliability of linear trend equations were assessed using the Fisher–Snedecor statistical test (F-test). The condition for significance is that the calculated

F-value $F_{calc.} = \frac{r^2}{1-r^2}(n-2)$ (where r is the correlation factor and n is the number of measurements) exceeds the critical F, $F_{critical}(\alpha; df_1; df_2)$, where α is the significance level and df are degrees of freedom (df_1 is the number of regressors, $df_1 = 1$, $df_2 = n - 2$). Only for the reforestation site are the significance and reliability of linear NDVI growth confirmed, and NDVI = 0.0234 + 0.0081·t (where t is 1 year after fire time), with an $r = 0.872$ correlation factor at all four standard significance levels: $\alpha = \{0.10; 0.05; 0.01; 0.001\}$.

The NDVI = 0.0894 + 0.0026·t equation of the linear trend and $r = 0.553$ for a mixed forest are significant when $\alpha = \{0.10; 0.05\}$ and are insignificant when α drops to 0.01. The trend for a coniferous forest ($r = 0.138$) is insignificant in all instances. As can be seen in Figure 7a, linear trends of NDVI for the reforestation site and the reference mixed forest intersected in 2016. Then, there was a tendency toward the restoration of the main species, the pine. Judging by Figure 7a, the intersection of the linear trend of the reforestation area with the trend for the pine forest area is predicted to occur in 27 years (in 2030). This is almost twofold higher than similar estimates made for the growth of young pine trees on flat terrain in the same region, obtained earlier in [30]. This is due to, first of all, the difference in natural and climatic aspects (soil fertility and moisture, air temperature, wind direction and intensity, and terrain) and initial conditions (afforestation of agricultural lands/restoration of burnt forests).

Figure 7b presents the radar vegetation index, RVI, time series, and linear trends. Here, we can see that a slight positive RVI trend was observed on the reference sites, i.e., the volumetric heterogeneity of the forest (size and number of branches) increased. The rate of annual increase in forest heterogeneity on the reference site was 3.67- and 2.20-fold higher than for coniferous and mixed forests, respectively. The F-test has shown that the significance condition was fulfilled for the linear trend of the RVI = 1.027 + 0.011·t increase (where t is 1 year after fire time) with an $r = 0.743$ correlation factor when $\alpha = \{0.10; 0.05\}$. This condition was fulfilled for the linear trend of the RVI = 1.38 + 0.005·t increase with an $r = 0.594$ correlation factor only when $\alpha = 0.10$. This condition corresponded to a mixed forest. For the coniferous forest, this trend was insignificant at all significance levels. This was evidence that the volume of aboveground biomass at this reference site could be considered stable over 13 years of radar measurements. Linear trends in Figure 7b suggest that if the growth rate of the radar RVI index in the control area of reforestation is maintained, the forest condition will reach the pre-fire level 41 years after the fire that took place in 2003.

The following results have been obtained using the proposed method of post-fire reforestation based on combining the optical and radar vegetation indices for 2016–2020 (13–18 years after the forest fire; see Figure 6):

- The average degree of total post-fire reforestation, the DRI, is equal to 0.29 (the DRI is equal to 1, or 100%, for the reference pine forest). The DRI increases at an average rate of 1.45% per year (DRI = 0.0145·t + 0.1386 with $r^2 = 0.63$). The estimated time to reach the level of the reference pine forest is 60 years (at a constant growth rate);
- Average projective cover by young pine trees; RSI_{pine} is equal to 0.35 (the RSI is equal to 1, or 100% for the reference pine forest). The RSI increases at an average rate of 7.12% per year (RSI = 0.0712·t − 0.2472 with $r^2 = 0.89$. The estimated time of the projective cover restoration is about 18 years after the fire.

Thus, the following estimates of predicted forest restoration after the fire that took place in the study area in 2003 were obtained: (1) 27 years, using NDVI only; (2) 41 years, using RVI only; and (3) 60 years, using the proposed combined method. The difference of more than twofold in the estimates by the first and third methods is due to the fact that the increase in projective cover of forest vegetation occurs much faster than complete restoration, taking into account the growth of biomass of trunks and trees. The species composition of pine is restored faster (18 years). In situ observations in the region confirm this: birch, aspen, and shrubs grow first, and then pine appears and becomes the main species.

The RVI-based estimate, to a greater extent, characterizes the moment when the aboveground biomass reaches the saturation threshold during L-band radar sensing. When

the saturation threshold is reached, it becomes difficult to register the increase in the biomass of trees, and the biomass dynamics will be lessened.

An analysis of archive in situ data for the studied region has shown that the maximum restoration period (60 years) corresponds to the average period of natural reforestation [16]. In some cases, after an abnormal burning of a forest along with fertile soil, this period may increase.

Therefore, the graph-based NDVI-RVI estimation method characterizes the dynamics of a young forest more accurately and completely compared to methods based on the use of only multispectral optical images or only L-band radar data. Generally, when taking into account the dynamics of forest canopy coverage and the biomass of the trunks and branches of young trees, an integral assessment effect appears. This makes it possible to more accurately compare their biophysical parameters with those of reference forest areas. As a result, the forest restoration time estimate has significantly improved.

6. Conclusions

The method for the comprehensive assessment of young forest status and the dynamics for quantitative and qualitative assessment of the degree of general reforestation and the degree of restoration of the main pine species (or its substitution with other species) are proposed here. In addition to a more accurate assessment of reforestation time compared with conventional separate analyses of multispectral optical imagery and radar data, the advantages of the proposed method are better visualization and the online availability of the involved remote sensing data.

Taking into account the above, specialists in various areas of expertise will be able to use this method to monitor reforestation/afforestation processes around the world. In turn, this will make it possible to use the proposed method to create a unified approach for estimating carbon sequestration by young trees in boreal forests. Moreover, the predicted time of reforestation after cuttings and fires, as well as agricultural land afforestation time, can be used for the classification of both a young forest with a high biomass buildup rate and high carbon absorbability and a mature forest with a lesser biomass buildup rate and carbon absorbability. Very useful information about changes in forest species composition can also be obtained. These data can be used to evaluate the health of boreal forests, where there is a higher potential for coniferous species to increase biomass than deciduous species. Thus, a new method has been proposed that will make it possible to refine global maps of carbon sequestration by boreal forests based on the identification and subsequent monitoring of reforestation/afforestation areas using satellite optical and radar data.

Author Contributions: Conceptualization, V.B. and T.C.; methodology, V.B., T.C. and I.K.; software, I.K. and A.D.; validation, T.C., I.K. and A.D.; formal analysis, V.B., T.C., I.K. and A.D.; investigation, V.B., T.C., I.K. and A.D.; data curation, A.D.; writing—original draft preparation, V.B., T.C. and I.K.; writing—review and editing, V.B., T.C. and A.D.; visualization, A.D. and I.K.; supervision, V.B. All authors have read and agreed to the published version of the manuscript.

Funding: The research was carried out within the state assignment of the Ministry of Science and Higher Education of the Russian Federation No. 1023032200011-7-2.7.4.

Data Availability Statement: All the data used are available in Google Earth Engine Data Catalog.

Acknowledgments: The authors are grateful to Arcadiy Baltukhaev for their participation in field data collection.

Conflicts of Interest: The authors declare no conflicts of interest.

References

1. Bellassen, V.; Luyssaert, S. Carbon sequestration: Managing forests in uncertain times. *Nature* **2014**, *506*, 153–155. [CrossRef] [PubMed]
2. Jiang, M.; Medlyn, B.E.; Drake, J.E.; Duursma, R.A.; Anderson, I.C.; Barton, C.V.M.; Boer, M.M.; Carrillo, Y.; Castañneda-Gómez, L.; Collins, L.; et al. The fate of carbon in a mature forest under carbon dioxide enrichment. *Nature* **2020**, *580*, 227–231. [CrossRef] [PubMed]

3. Pinnington, E.M.; Casella, E.; Dance, S.L.; Lawless, A.S.; Morison, J.I.; Nichols, N.K.; Wilkinson, M.; Quaife, T.L. Understanding the effect of disturbance from selective felling on the carbon dynamics of a managed woodland by combining observations with model predictions. *J. Geophys. Res. Biogeosci.* **2017**, *122*, 886–902. [CrossRef]
4. Pugh, T.A.M.; Lindeskog, M.; Smith, B.; Poulter, B.; Arneth, A.; Haverd, V.; Calle, L. Role of forest regrowth in global carbon sink dynamics. *Proc. Natl. Acad. Sci. USA* **2019**, *116*, 4382–4387. [CrossRef]
5. Chazdon, R.L.; Broadbent, E.N.; Rozendaal, D.M.A.; Bongers, F.; Zambrano, A.M.A.; Aide, T.M.; Balvanera, P.; Becknell, J.M.; Boukili, V.; Brancalion, P.H.S.; et al. Carbon sequestration potential of second-growth forest regeneration in the Latin American tropics. *Sci. Adv.* **2016**, *2*, e1501639. [CrossRef]
6. Ivanov, A.Y.; Durmanov, N.D.; Orlov, M.P.; Piksendeev, K.V.; Rovnov, Y.E.; Luksha, P.O.; Makarov, I.A.; Ptichnikov, A.V.; Stepanov, I.A.; Kharchenko, M.M.; et al. *Bitva za Klimat: Karbonovoye Zemledeliye Kak Stavka Rossii (Battle for Climate: Carbon Farming Like Russia's Bet)*; Expert Report; HSE University Publication: Moscow, Russia, 2021; 120p. (In Russian)
7. Erbaugh, J.T.; Pradhan, N.; Adams, J.; Oldekop, J.A.; Agrawal, A.; Brockington, D.; Pritchard, R.; Chhatre, A. Global forest restoration and the importance of prioritizing local communities. *Nat. Ecol. Evol.* **2020**, *4*, 1472–1476. [CrossRef]
8. Koch, A.; Kaplan, J.O. Tropical forest restoration under future climate change. *Nat. Clim. Chang.* **2022**, *12*, 279–283. [CrossRef]
9. Bondur, V.G.; Gordo, K.A.; Kladov, V.L. Spacetime distributions of wildfire areas and emissions of carbon-containing gases and aerosols in northern Eurasia according to satellite-monitoring data. *Izv. Atmos. Ocean. Phys.* **2017**, *53*, 859–874. [CrossRef]
10. Bondur, V.G.; Gordo, K.A. satellite monitoring of burnt-out areas and emissions of harmful contaminants due to forest and other wildfires in Russia. *Izv. Atmos. Ocean. Phys.* **2018**, *54*, 955–965. [CrossRef]
11. Jung, M.; Lesiv, M.; Warren-Thomas, E.; Shchepashchenko, D.; See, L.; Fritz, S. The importance of capturing management in forest restoration targets. *Nat. Sustain.* **2023**, *6*, 1717. [CrossRef]
12. Loupian, E.; Burtsev, M.; Proshin, A.; Kashnitskii, A.; Balashov, I.; Bartalev, S.; Konstantinova, A.; Kobets, D.; Radchenko, M.; Tolpin, V.; et al. Usage Experience and Capabilities of the VEGA-Science System. *Remote Sens.* **2022**, *14*, 77. [CrossRef]
13. The JJ-FAST System. Available online: https://www.eorc.jaxa.jp/jjfast/system.html (accessed on 4 January 2024).
14. Koyama, C.N.; Watanabe, M.; Hayashi, M.; Shimada, M.; Kobayashi, K.; Tadono, T. Advancements in Global Forest Monitoring Research Founded on ALOS-2 Long-Term Pantropical Land Observation. In Proceedings of the IGARSS 2022—2022 IEEE International Geoscience and Remote Sensing Symposium, Kuala Lumpur, Malaysia, 17 July 2022; pp. 4445–4448. [CrossRef]
15. Watanabe, M.; Koyama, C.N.; Hayashi, M.; Nagatani, I.; Tadono, T.; Shimada, M. Refined algorithm for forest early warning system with ALOS-2/PALSAR-2 ScanSAR data in tropical forest regions. *Remote Sens. Environ.* **2021**, *265*, 112643. [CrossRef]
16. Bondur, V.; Chimitdorzhiev, T.; Kirbizhekova, I.; Dmitriev, A. Estimation of Postfire Reforestation with SAR Polarimetry and NDVI Time Series. *Forests* **2022**, *13*, 814. [CrossRef]
17. Cavalli, A.; Francini, S.; Cecili, G.; Cocozza, C.; Congedo, L.; Falanga, V.; Spadoni, G.L.; Maesano, M.; Munafò, M.; Chirici, G.; et al. Afforestation monitoring through automatic analysis of 36-years Landsat Best Available Composites. *Forests* **2022**, *15*, 220–228. [CrossRef]
18. Cavalli, A.; Francini, S.; McRoberts, R.E.; Falanga, V.; Congedo, L.; De Fioravante, P.; Maesano, M.; Munafò, M.; Chirici, G.; Scarascia Mugnozza, G. Estimating Afforestation Area Using Landsat Time Series and Photointerpreted Datasets. *Remote Sens.* **2023**, *15*, 923. [CrossRef]
19. Ershov, D.V.; Gavrilyuk, E.A.; Koroleva, N.V.; Belova, E.I.; Tikhonova, E.V.; Shopina, O.V.; Titovets, A.V.; Tikhonov, G.N. Natural Afforestation on Abandoned Agricultural Lands during Post-Soviet Period: A Comparative Landsat Data Analysis of Bordering Regions in Russia and Belarus. *Remote Sens.* **2022**, *14*, 322. [CrossRef]
20. The BAP Library. Available online: https://code.earthengine.google.com/?accept_repo=users/sfrancini/bap (accessed on 4 January 2024).
21. Landsat 5 TM Collection 1 Tier 1 32-Day NDVI Composite. Available online: https://developers.google.com/earth-engine/datasets/catalog/LANDSAT_LT05_C01_T1_32DAY_NDVI (accessed on 4 January 2024).
22. Landsat 8 Collection 1 Tier 1 32-Day NDVI Composite. Available online: https://developers.google.com/earth-engine/datasets/catalog/LANDSAT_LC08_C01_T1_32DAY_NDVI (accessed on 4 January 2024).
23. Landsat 8 Collection 1 Tier 1 32-Day NBRT Composite. Available online: https://developers.google.com/earth-engine/datasets/catalog/LANDSAT_LC08_C01_T1_32DAY_NBRT (accessed on 4 January 2024).
24. Chuvieco, E.; Congalton, R. Mapping and inventory of forest fires from digital processing of tm data. *Geocarto Intern.* **1988**, *3*, 41–53. [CrossRef]
25. Alcaras, E.; Costantino, D.; Guastaferro, F.; Parente, C.; Pepe, M. Normalized Burn Ratio Plus (NBR+): A New Index for Sentinel-2 Imagery. *Remote Sens.* **2022**, *14*, 1727. [CrossRef]
26. Global PALSAR-2/PALSAR Yearly Mosaic, Version 1. Available online: https://developers.google.com/earth-engine/datasets/catalog/JAXA_ALOS_PALSAR_YEARLY_SAR (accessed on 4 January 2024).
27. Yadav, V.P.; Prasad, R.; Bala, R.; Srivastava, P.K.; Vanama, V.S.K. Appraisal of Dual Polarimetric Radar Vegetation Index in First Order Microwave Scattering Algorithm Using Sentinel-1A (C-Band) and ALOS 2 (L-Band) SAR Data. *Geocarto Intern.* **2022**, *37*, 6232–6250. [CrossRef]
28. Park, S.-E. Variations of Microwave Scattering Properties by Seasonal Freeze/Thaw Transition in the Permafrost Active Layer Observed by ALOS PALSAR Polarimetric Data. *Remote Sens.* **2015**, *7*, 17135–17148. [CrossRef]

29. Park, S.-E.; Jung, Y.K.; Kim, H.-C. Monitoring permafrost changes in central Yakutia using optical and polarimetric SAR data. *Remote Sens. Environ.* **2022**, *274*, 112989. [CrossRef]
30. Dmitriev, A.V.; Chimitdorzhiev, T.N.; Dobrynin, S.I.; Khudaiberdieva, O.; Kirbizhekova, I. Optical-microwave diagnostics of agricultural land afforestation. *Sovrem. Probl. Distantsionnogo Zondirovaniya Zemli Kosmosa* **2022**, *19*, 168–180. [CrossRef]

Disclaimer/Publisher's Note: The statements, opinions and data contained in all publications are solely those of the individual author(s) and contributor(s) and not of MDPI and/or the editor(s). MDPI and/or the editor(s) disclaim responsibility for any injury to people or property resulting from any ideas, methods, instructions or products referred to in the content.